Euro. Jnl of Applied Mathematics (2005), *vol.* 16, *pp.* 601–619.
doi:10.1017/S0956792505006443 Printed in the United Kingdom

Free surface flows past surfboards and sluice gates

B. J. BINDER and J.-M. VANDEN-BROECK

School of Mathematics, University of East Anglia, Norwich NR4 7TJ, UK
email: {b.binder,J.Vanden-broeck}@uea.ac.uk

(*Received 14 January 2005; revised 19 July 2005*)

Free surface potential flows past surfboards and sluice gates are considered. The problem is solved numerically by boundary integral equation methods. In addition weakly nonlinear solutions are presented. It is shown among the six possible types of steady flows, only three exist. The physical relevance of these solutions is discussed in terms of the radiation condition (which requires that there is no energy coming from infinity). In particular, it is shown there are no steady subcritical flows which satisfy the radiation condition. Similarly there are no solutions for the flow under a sluice gate.

1 Introduction

Many applications involve free surface flows past surface piercing objects. Examples include the flow due to a moving ship and the flow under a sluice gate.

An idealised two-dimensional configuration is sketched in Figure 1(a). Here the object is a flat plate BC inclined at an angle σ_c with the horizontal. The fluid is inviscid and incompressible and the flow is steady, irrotational and bounded below by the horizontal bottom $A'D'$. The free surfaces AB and CD are assumed to separate tangentially from the plate at the points B and C. A system of Cartesian coordinates (x^*, y^*) is defined with the origin on the bottom and the y^*-axis passing through the separation point B. Gravity acts in the negative y^*-direction. We assume that the flow approaches a uniform stream with constant velocity U and constant depth H as $x^* \to \infty$. The dimensionless downstream Froude number can then be defined as

$$F = \frac{U}{\sqrt{gH}}, \tag{1.1}$$

where g is the acceleration due to gravity. The flow is referred to as subcritical if $F < 1$ and as supercritical if $F > 1$. Linear theory predicts that supercritical flows are waveless. Far upstream the flow can be uniform or possess a train of waves. When it is uniform, we introduce the upstream Froude number

$$F^* = \frac{V}{\sqrt{gD}} \tag{1.2}$$

where V and D are the uniform velocity and uniform depth far upstream.

The configuration of Figure 1(a) describes the flow due to a plate BC moving at a constant horizontal velocity U when viewed in a frame of reference moving with the plate. It also models the free surface flow under a sluice gate or past a 'surfboard'.

As we shall see, the dynamic boundary condition and the conservation of mass restrict the possible flows to six types: subcritical flows with one train of waves ($F < 1$, waves as $x^* \to -\infty$, no waves as $x^* \to \infty$), subcritical with two trains of waves (waves as $x^* \to \pm\infty$), waveless subcritical flows ($F = F^* < 1$, no waves as $x^* \to \pm\infty$), supercritical flows ($F = F^* > 1$, no waves as $x^* \to \pm\infty$), critical flows ($F^* < 1$, $F > 1$, no waves as $x^* \to \pm\infty$) and generalised critical flows ($F > 1$ and waves as $x^* \to -\infty$).

The subcritical flows describe the free surface flow due to a plate moving at a constant velocity U at the surface of the fluid, when viewed in a frame of reference moving with the plate. We note that subcritical flows with waves have to satisfy the radiation condition (which requires that no energy comes from infinity). Therefore only the subcritical flow with one train of waves satisfies the radiation condition provided that the direction of the flow (i.e. the direction of the arrow in Figure 1(a)) is reversed. This can be done since potential flows are reversible.

The critical flows describe the flow under a sluice gate. This is a classical problem of hydrodynamics which has been considered by many previous investigators (see, for example, Binnie [4], Benjamin [2], Frangmeier & Strelkoff [9], Lamb [11], Chung [6], Vanden-Broeck [14], Budden & Norbury [5] and Asavanant & Vanden-Broeck [1]).

The supercritical flows were considered before by Vanden-Broeck & Keller [13]. They are referred to as 'surfing flows' because the level of the plate is higher than the level of the free surface at $x^* \to \pm\infty$.

In this paper, we show that out of the six types of flows, only the supercritical flows, the subcritical flows with two trains of waves and the generalised critical flows exist. This is established by careful numerical computations using boundary integral equation methods and by analytical methods based on weakly nonlinear theories. These results imply in particular the nonexistence of subcritical flows satisfying the radiation condition. Similarly there are no solutions for the flow under a sluice gate which satisfies the radiation condition (there is always a train of waves as $x^* \to -\infty$). This finding is consistent with the previous results of Vanden-Broeck [14], who considered the case of a vertical sluice gate.

The formulation and numerical procedure for flow past an inclined sluice gate or surfboard is given in § 2. Nonlinear and weakly nonlinear free surface profiles for surfboards and sluice gates presented and discussed in § 3. Finally, concluding remarks are made in § 4.

2 Formulation

Consider the steady two-dimensional irrotational flow of an incompressible inviscid fluid bounded below by the horizontal bottom $A'D'$ (see Figure 1(a)). The flow is bounded above by a wall BC and two free surfaces AB and CD. The equations of the free surfaces AB and CD can be written as $y^* = H + \eta^*(x^*)$ (see Figure 1(a)). The function $\eta^*(x^*)$ is uniquely defined by requiring $\eta^*(x^*) \to 0$ as $x^* \to \infty$.

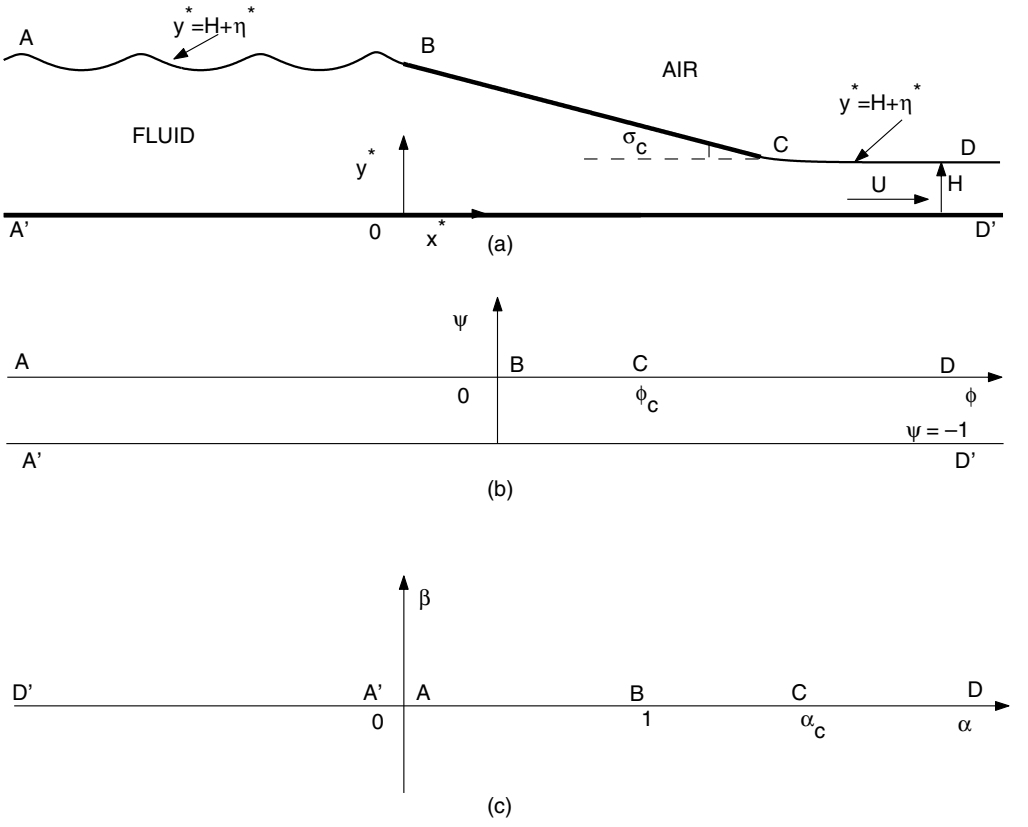

FIGURE 1. (a) Sketch of flow in physical coordinates (x^*, y^*). (b) Sketch of flow in the plane of the complex potential (f-plane). (c) Sketch of flow in the lower half-plane (ζ-plane).

The dynamic boundary condition on the free surfaces AB and CD gives

$$\frac{1}{2}(u^{*2} + v^{*2}) + g\eta^*(x^*) = \frac{1}{2}U^2 + gH \quad \text{on} \quad y^* = H + \eta^*(x^*) \tag{2.1}$$

where u^* and v^* are the horizontal and vertical components of the velocity. Here, we have used the conditions $u^* \to U$, $v^* \to 0$, $\eta^*(x^*) \to 0$ as $x^* \to \infty$, to evaluate the Bernoulli constant on the right hand side of (2.1).

As mentioned in the introduction, the flow as $x^* \to -\infty$, can be characterized either by a uniform stream with constant velocity V and constant depth D or by a train of waves. When the flow as $x^* \to -\infty$ is uniform a relation between F and D/H can be derived in the following way. First the conservation of mass implies

$$VD = UH. \tag{2.2}$$

Next (2.1) evaluated in the limit $x^* \to -\infty$, yields

$$\frac{1}{2}V^2 + gD = \frac{1}{2}U^2 + gH. \tag{2.3}$$

Combining (2.2) and (2.3) gives the relations

$$F^2\left[\frac{D^2}{H^2}-1\right]=\frac{2D^2}{H^2}\left(\frac{D}{H}-1\right) \tag{2.4}$$

and

$$F^{*2}\left[\frac{H^2}{D^2}-1\right]=\frac{2H^2}{D^2}\left(\frac{H}{D}-1\right) \tag{2.5}$$

Equations (2.4) and (2.5) are satisfied if either

$$H=D, \quad F=F^* \tag{2.6}$$

or

$$F=\frac{2}{\left(\frac{H}{D}\right)^2+\frac{H}{D}}, \quad F^*=\frac{2}{\left(\frac{D}{H}\right)^2+\frac{D}{H}} \tag{2.7}$$

Assuming without loss of generality $D > H$, equations (2.7) implies that $F > 1$ and $F^* < 1$. From (2.6) and (2.7) we see that there are three possible types of solutions with a uniform stream as $x^* \to \pm\infty$. The first is a (waveless) supercritical flow with $F = F^* > 1$. The second is a waveless subcritical flow with $F = F^* < 1$. The third is a waveless critical flow with $F^* < 1$ and $F > 1$.

There are in addition three possible types of solutions with a train of waves as $x^* \to -\infty$. The first is a subcritical flow with $F < 1$ (no waves as $x^* \to \infty$) and a train of waves as $x^* \to -\infty$. The second is a subcritical flow with two trains of waves as $x^* \to \pm\infty$. The third is a generalised critical flow with $F > 1$ (no waves as $x^* \to \infty$) and a train of waves as $x^* \to -\infty$.

Therefore there are six types of solutions. As we shall see only the supercritical flows, the subcritical flows with two trains of waves and the generalised critical flows exist. In the next subsection we give details of the formulation of the boundary integral equation method for the fully nonlinear problem.

2.1 Boundary integral equation method

We define dimensionless variables by taking H as the reference length and U as the reference velocity. Thus we define the dimensionless variables $(x, y) = (x^*, y^*)/H$. The free surfaces AB and CD are then described by $y = 1 + \eta(x)$, where $\eta = \eta^*/H$. The dimensionless horizontal and vertical components of the velocity are u and v respectively.

The dynamic boundary condition (2.1) is now rewritten as

$$\frac{1}{2}(u^2+v^2)+\frac{1}{F^2}y=\frac{1}{2}+\frac{1}{F^2} \tag{2.8}$$

where F is the Froude number defined by (1.1).

The nonlinear problem can be reduced to a problem in complex analysis. We first introduce the potential function ϕ and stream function ψ. We then define the complex potential, $f = \phi + i\psi$, and complex velocity, $w = \frac{df}{dz} = u - iv$. Without loss of generality we choose $\psi = 0$ on the free surface streamline, $ABCD$ and $\phi = 0$ at the separation point B. We denote the value of ϕ at the separation point C, by ϕ_c. It follows from the conservation of mass, that $\psi = -1$ on the bottom of the channel $A'D'$. The fluid domain in the complex f-plane is the strip $-1 < \psi < 0$, see Figure 1(b).

We map the strip $-1 < \psi < 0$ onto the lower half ζ-plane by the transformation

$$\zeta = \alpha + i\beta = e^{\pi f}. \tag{2.9}$$

The flow configuration in the ζ-plane is shown in Figure 1(c).

We define the function $\tau - i\theta$ by

$$u - iv = e^{\tau - i\theta} \tag{2.10}$$

and we apply Cauchy integral equation formula to the function $\tau - i\theta$ in the ζ-plane with a contour consisting of the α axis and a semi circle of arbitrary large radius in the lower half plane. Since $\tau - i\theta \to 0$ as $|\zeta| \to \infty$, there is no contribution from the half circle and we obtain (after taking the real part)

$$\tilde{\tau}(\alpha) = \frac{1}{\pi} \int_{-\infty}^{\infty} \frac{\tilde{\theta}(\alpha_0)}{\alpha_0 - \alpha}\, d\alpha_0, \tag{2.11}$$

where $\tilde{\tau}(\alpha)$ and $\tilde{\theta}(\alpha)$ are the values of τ and θ on the α-axis. The integral in (2.11) is a Cauchy principal value.

The kinematic boundary conditions on the bottom of the channel and free surface rigid plate BC imply

$$\tilde{\theta}(\alpha) = 0 \quad \text{for} \quad \alpha < 0 \tag{2.12}$$

and

$$\tilde{\theta}(\alpha) = -\sigma_c \quad \text{for} \quad 1 < \alpha < \alpha_c. \tag{2.13}$$

Here $\alpha_c = e^{\pi\phi_c}$. Substituting (2.12) and (2.13) in (2.11) gives

$$\tilde{\tau}(\alpha) = -\frac{\sigma_c}{\pi} \ln \frac{|\alpha_c - \alpha|}{|1 - \alpha|} + \frac{1}{\pi} \int_0^1 \frac{\theta(\alpha_0)}{\alpha_0 - \alpha}\, d\alpha_0 + \frac{1}{\pi} \int_{\alpha_c}^{\infty} \frac{\theta(\alpha_0)}{\alpha_0 - \alpha}\, d\alpha_0. \tag{2.14}$$

We assume that $\alpha > 0$ (i.e. that α corresponds to points on the free surface) and rewrite (2.14) in terms of ϕ by using the change of variables

$$\alpha = e^{\pi\phi}, \quad \alpha_0 = e^{\pi\phi_0}. \tag{2.15}$$

This gives

$$\tau(\phi) = -\frac{\sigma_c}{\pi} \ln \frac{|e^{\pi\phi_c} - e^{\pi\phi}|}{|1 - e^{\pi\phi}|} + \int_{-\infty}^{0} \frac{\theta(\phi_0) e^{\pi\phi_0}}{e^{\pi\phi_0} - e^{\pi\phi}} d\phi_0 + \int_{\phi_c}^{\infty} \frac{\theta(\phi_0) e^{\pi\phi_0}}{e^{\pi\phi_0} - e^{\pi\phi}} d\phi_0 \tag{2.16}$$

Here $\tau(\phi) = \tilde{\tau}(e^{\pi\phi})$ and $\theta(\phi) = \tilde{\theta}(e^{\pi\phi})$.

Integrating the identity

$$x_\phi + iy_\phi = \frac{1}{u - iv} = e^{-\tau + i\theta} \tag{2.17}$$

and equating real and imaginary parts we can obtain parametric relations for the shape of the free surfaces AB and CD. The equations for the upstream free surface AB are

$$x(\phi) = \int_0^{\phi} e^{-\tau(\phi_0)} \cos\theta(\phi_0) d\phi_0 \quad \text{for} \quad -\infty < \phi < 0 \tag{2.18}$$

and

$$y(\phi) = y(0) + \int_0^{\phi} e^{-\tau(\phi_0)} \sin\theta(\phi_0)\, d\phi_0 \quad \text{for} \quad -\infty < \phi < 0. \tag{2.19}$$

Those on the downstream free surface CD are

$$x(\phi) = x(\phi_c) + \int_{\phi_c}^{\phi} e^{-\tau(\phi_0)} \cos\theta(\phi_0)\, d\phi_0 \quad \text{for} \quad \phi_c < \phi < \infty \tag{2.20}$$

and

$$y(\phi) = 1 + \int_{\infty}^{\phi} e^{-\tau(\phi_0)} \sin\theta(\phi_0)\, d\phi_0 \quad \text{for} \quad \phi_c < \phi < \infty. \tag{2.21}$$

We will define $y(0)$ in (2.19) for particular types of nonlinear solutions in section § 3.

Another equation on the free surfaces is obtained by substituting (2.10) into (2.8). This yields

$$e^{2\tau} + \frac{2}{F^2} y = 1 + \frac{2}{F^2}. \tag{2.22}$$

Equations (2.16), (2.19), (2.21) and (2.22) define a nonlinear integral equation for the unknown function $\theta(\phi)$ on the free surfaces $-\infty < \phi < 0$ and $\phi > \phi_c$. We note that the values of $x(\phi)$ and $x(\phi_c)$ in (2.18) and (2.20) are not needed to calculate $\theta(\phi)$. Therefore they can be evaluated after a converged solution has been obtained.

2.2 Numerical scheme

We solve the integral equation defined by (2.16), (2.19), (2.21) and (2.22) numerically. The numerical procedure follows Vanden-Broeck [14], Binder *et al.* [3] and others. We first introduce the equally spaced mesh points in the potential function ϕ:

$$\phi_I^U = -(I-1)\Delta_1, \quad I = 1, \ldots, N_1 \tag{2.23}$$

and

$$\phi_I^D = \phi_c + (I-1)\Delta_2, \quad I = 1, \ldots, N_2, \tag{2.24}$$

where $\Delta_1 > 0$ and $\Delta_2 > 0$ are the mesh sizes. The corresponding unknowns are

$$\theta_I^U = \theta(\phi_I^U), \quad I = 1, \ldots, N_1 \tag{2.25}$$

and

$$\theta_I^D = \theta(\phi_I^D), \quad I = 1, \ldots, N_2. \tag{2.26}$$

Since the flow separates tangentially from the sluice gate or surfboard $\theta_1^U = \theta_1^D = -\sigma_c$. There are then $N_1 + N_2 - 2$ unknowns θ_I^U and θ_I^D.

The values $\tau_{I+1/2}^U$ and $\tau_{I+1/2}^D$ of $\tau(\phi)$ are evaluated at the midpoints

$$\phi_{I+1/2}^U = \frac{\phi_I^U + \phi_{I+1}^U}{2}, \quad I = 1, \ldots, N_1 - 1 \tag{2.27}$$

and

$$\phi^D_{I+1/2} = \frac{\phi^D_I + \phi^D_{I+1}}{2}, \quad I = 1, \ldots, N_2 - 1 \tag{2.28}$$

by applying the trapezoidal rule to the integrals in (2.16) with summations over the points ϕ^U_I and ϕ^D_I. The symmetry of the quadrature and of the distribution of the points enable us to evaluate the Cauchy principal values as if they were ordinary integrals.

Following Hocking & Vanden-Broeck [10], the integrals in (2.16) are re-written as

$$\int_{\phi^U_{N_1}}^{0} \frac{(\theta(\phi_0) - \theta_{I+1/2})e^{\pi\phi_0}}{e^{\pi\phi_0} - e^{\pi\phi_{I+1/2}}}\, d\phi_0 + \frac{\theta_{I+1/2}}{\pi} \ln \frac{|1 - e^{\pi\phi_{I+1/2}}|}{|e^{\pi\phi^U_{N_1}} - e^{\pi\phi_{I+1/2}}|} \tag{2.29}$$

and

$$\int_{\phi_c}^{\phi^D_{N_2}} \frac{(\theta(\phi_0) - \theta_{I+1/2})e^{\pi\phi_0}}{e^{\pi\phi_0} - e^{\pi\phi_{I+1/2}}}\, d\phi_0 + \frac{\theta_{I+1/2}}{\pi} \ln \frac{|e^{\pi\phi^D_{N_2}} - e^{\pi\phi_{I+1/2}}|}{|e^{\pi\phi_c} - e^{\pi\phi_{I+1/2}}|} \tag{2.30}$$

before applying the trapezoidal rule. The values $\theta^U_{I+1/2}$, $\theta^D_{I+1/2}$ of θ at the mesh points (2.27), (2.28) are evaluated in terms of the unknowns (2.25) and (2.26) by interpolation formulas.

Now $y^U_I = y(\phi^U_I)$ and $y^D_I = y(\phi^D_I)$ can be evaluated recursively using (2.19) and (2.21). This yields

$$y^U_1 = y(0)$$

$$y^U_I = y^U_{I-1} - e^{[-\tau^U_{I-1/2}]} \sin[\theta^U_{I-1/2}]\Delta_1, \quad I = 2, \ldots, N_1; \tag{2.31}$$

$$y^D_{N_2} = 1,$$

$$y^D_I = y^D_{I+I} - e^{[-\tau^D_{I+1/2}]} \sin[\theta^D_{I+1/2}]\Delta_2, \quad I = N_2 - 1, \ldots, 1. \tag{2.32}$$

The values (2.31) and (2.32) are used to evaluate $y(\phi)$ at the midpoints (2.27) and (2.28) by interpolation formulas.

Now (2.22) can be satisfied at the midpoints (2.27) and (2.28). This yields a system of $N_1 + N_2 - 2$ nonlinear algebraic equations. We shall refer to this system of $N_1 + N_2 - 2$ equations as the system [*].

Another equation can be derived by fixing the length L of the plate BC. Using (2.13) and the identity (2.17) gives

$$\frac{\partial y}{\partial \phi} = -e^{-\tau} \sin[\sigma_c] \quad \text{on} \quad 0 < \phi < \phi_c. \tag{2.33}$$

Numerically integrating (2.33) yields the length L of the plate BC in terms of the unknowns and the extra equation is then

$$y^U_1 - y^D_1 - L \sin[\sigma_c] = 0. \tag{2.34}$$

Further details on the schemes depend on the type of flow calculated and will be given in section § 3.

2.3 Weakly nonlinear theory

The determination of the number of independent parameters needed to obtain a unique solution to a free surface problem is often delicate and counter intuitive. It can be found by careful numerical experimentation (fixing too many or too few parameters fails to yield convergence). An alternative approach is to perform a weakly nonlinear analysis in the phase plane. This second approach has the advantage of allowing a systematic determination of all the possible solutions (within the range of validity of the weakly nonlinear theory). Both approaches are used in this paper for flows past sluice gates and surfboards.

As we shall see, the Korteweg de Vries (KdV) equation can be used to model the flow past an inclined sluice gate or surfboard in a channel. Since the present paper deals with steady solutions, we only consider the steady KdV equation. Our approach follows the work of Shen [12], Dias & Vanden-Broeck [8] and Binder *et al.* [3], who derived forced Korteweg de Vries equation to model the flow past an obstacle on the bottom of the channel.

The classical derivation of the Korteweg de Vries equation is based on long wavelength asymptotics. Thus if L denotes a typical horizontal lengthscale and H is the constant depth as $x^* \to \infty$, we introduce the small parameter $\epsilon = (H/L)^2 \ll 1$, the dimensionless spatial variables $(\acute{x}, \acute{y}) = (\epsilon^{1/2}x^*, y^*)/H$ and the free-surface elevation $\epsilon\acute{\eta} = \eta^*/H$. The Froude number F is written as $F = 1 + \epsilon\mu$.

Substituting expansions in powers of ϵ into the exact potential equations (rewritten in terms of the new scaled variables), the KdV equation is derived by equating coefficients of the powers of ϵ. The KdV equation (rewritten in terms of the variables $x = \epsilon^{-1/2}\acute{x}$ and $\eta = y - 1 = \epsilon\acute{\eta}$ used in the nonlinear computations) is

$$\eta_{xx} + \frac{9}{2}\eta^2 - 6(F-1)\eta = 0. \tag{2.35}$$

Equation (2.35) is valid when $F \sim 1$ and $|\eta| \ll 1$. It can therefore be expected to describe the free surfaces AB and CD of Figure 1(a) when $F \sim 1$ and $\sigma_c \ll 1$.

Multiplying (2.35) by η_x and integrating yields

$$\eta_x^2 = 6(F-1)\eta^2 - 3\eta^3 + C. \tag{2.36}$$

Here C is a constant of integration.

If we extend the definition of $\eta(x)$ to denote the elevation of the complete streamline $ABCD$ we can write

$$\eta_x = -\tan[\sigma_c] \quad \text{on} \quad BC \tag{2.37}$$

Weakly nonlinear solutions of the flow of Figure 1(a) are solutions of (2.36) and (2.37). It is convenient to describe them in the phase plane where we plot values of η_x versus η.

There are two fixed points $\eta = 0$, $\eta_x = 0$ and $\eta = 4/3(F-1)$, $\eta_x = 0$. Classification of the fixed points depend on whether $F > 1$ (supercritical) or $F < 1$ (subcritical). For supercritical flow $F > 1$, there is a centre at $\eta = 4/3(F-1)$, $\eta_x = 0$ and a saddle point at $\eta = 0$, $\eta_x = 0$. For subcritical flow $F < 1$, there is a centre at $\eta = 0$, $\eta_x = 0$ and a saddle point at $\eta = \eta = 4/3(F-1)$, $\eta_x = 0$. Phase portraits with no disturbances for supercritical

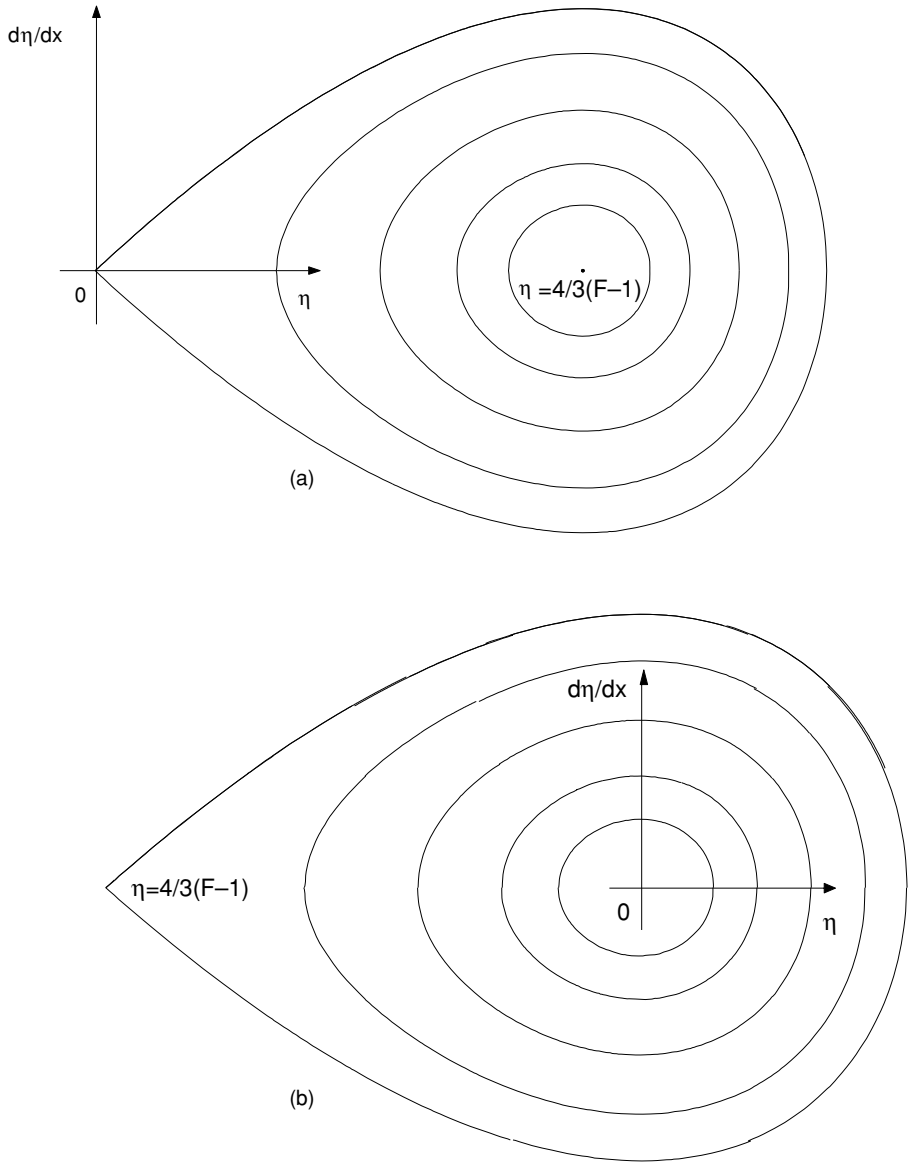

FIGURE 2. Weakly nonlinear phase portraits, $\frac{d\eta}{dx}$ versus η. (a) Supercritical flow, $F > 1$. There is a saddle point at $\eta = 0$, $\eta_x = 0$ and a centre at $\eta = 4/3(F-1)$, $\eta_x = 0$. (b) Subcritical flow, $F < 1$. There is a saddle point at $\eta = 4/3(F-1)$, $\eta_x = 0$ and a centre at $\eta = 0$, $\eta_x = 0$.

and subcritical flow are shown in Figures 2(a),(b). If there is a gate, (2.37) shows that we need to incorporate in the phase diagrams Figures 2(a),(b), horizontal jumps whose magnitude is equal to the difference of heights between the ends of the gate or surfboard. As we shall see in the next section, the resulting phase diagrams provide weakly nonlinear solutions for the flow configuration of Figure 1(a) which are valid for $F \approx 1$ and $\sigma_c \ll 1$.

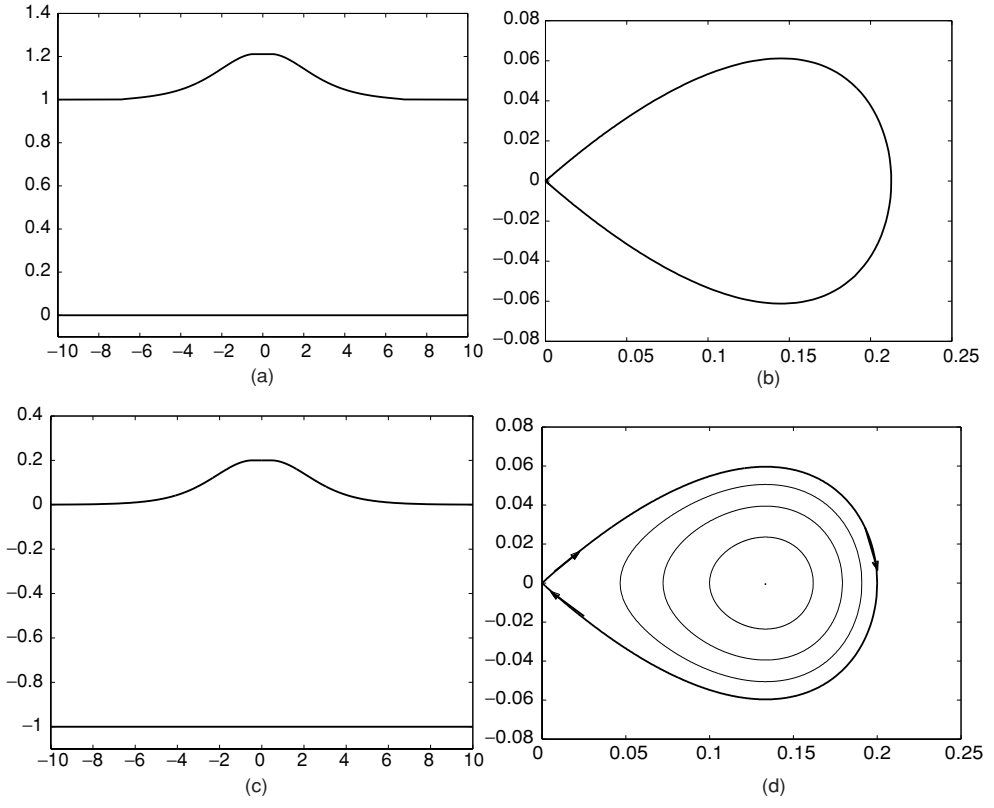

FIGURE 3. Supercritical flow for $F = 1.10$, $L = 1.00$ and $\sigma_c = 0.0$ (a) Fully nonlinear free surface profile, $\gamma = 0.21$ and $\phi_c = 0.80$. (b) Values of $\frac{dy}{dx} = \tan(\theta)$ versus $y - 1 = \eta$, showing the fully nonlinear phase trajectories for figure (a). (c) Weakly nonlinear profile, $\gamma = 0.20$. (d) Weakly nonlinear phase portrait for figure (c), $\frac{d\eta}{dx}$ versus η.

3 Results

In this section, we present fully nonlinear results and weakly nonlinear results for supercritical flows, subcritical flows and flows under a sluice gate. These results are described in three separate subsections.

3.1 Supercritical flows: flows past surfboards

Here we discuss nonlinear and weakly nonlinear free surface profiles for supercritical flows $F^* = F > 1$ past a plate of length L, see Figures 3(a), (c) and 4(a), (c). Since the plate is on top of the level of the flow in the far field, we refer to these flows as 'surfing flows' and to the plate as a 'surfboard'. The range of validity of the weakly nonlinear theory is established by comparing nonlinear and weakly nonlinear free surface profiles. Previously, Vanden-Broeck & Keller [13] computed nonlinear solutions using a method of series truncation. They found that for a horizontal surfboard ($\sigma_c = 0$), there is a two parameter family of solutions, whereas for an inclined board ($\sigma_c \neq 0$), there is a one

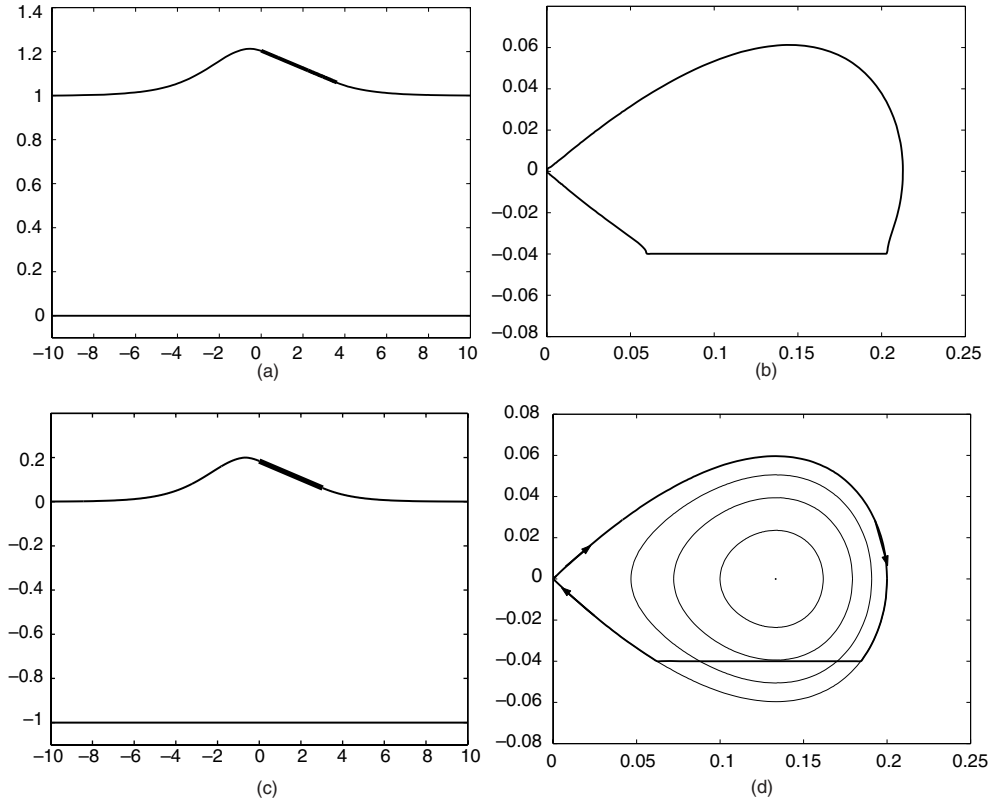

FIGURE 4. Supercritical flow for $F = 1.10$ and $\sigma_c = 2.30°$. (a) Fully nonlinear free surface profile, $\gamma = 0.20$ and $L = 3.59$. (b) Values of $\frac{dy}{dx} = \tan(\theta)$ versus $y - 1 = \eta$, showing the fully nonlinear phase trajectories for figure (a). (c) Weakly nonlinear profile, $\gamma = \eta_1 = 0.184$, $\eta_2 = 0.062$ and $L = 3.05$. (d) Weakly nonlinear phase portrait for figure (c), $\frac{d\eta}{dx}$ versus η.

parameter family of solutions. We recover these results by using our boundary integral equation method. In addition we explain the qualitative behaviour of the solutions (in particular, the number of parameters needed to determine uniquely solutions) by applying the weakly nonlinear theory. Finally new types of solutions are identified and discussed.

For the nonlinear computations we defined the height of the intersection of the upstream free surface with the surfboard as

$$y_1^U = y(0) = 1 + \gamma.$$

Here γ is the elevation of the point B on top of the level of the free surface at $x = \infty$ (see Figure 1(a)).

For a horizontal surfboard, $\sigma_c = 0$, a two parameter family of solutions was found. The parameters can be chosen as the downstream Froude number $F > 1$ and the length of the surfboard L (or ϕ_c). There are then $N_1 + N_2 - 1$ unknowns γ, θ_I^U, $I = 2, \ldots, N_1$, and θ_I^D, $I = 2, \ldots, N_2$. The system of equations [*] yields $N_1 + N_2 - 2$ nonlinear algebraic

equations and for a horizontal surfboard the last equation is

$$y_1^D = y(\phi_c) = 1 + \gamma.$$

This system of $N_1 + N_2 - 1$ equations with $N_1 + N_2 - 1$ unknowns can be solved using Newton's method for given values of $F > 1$ and L (or ϕ_c). We note that γ is the elevation of the horizontal plate or surfboard.

Figure 3(a) is a computed nonlinear profile for $F = 1.10$, $L = 1.00$ ($\phi_c = 0.80$) and $\gamma = 0.21$. Figure 3(c) is the weakly nonlinear profile for $F = 1.10$, $L = 1.00$ and $\gamma = 0.20$. Essentially the nonlinear profile, Figure 3(a) and weakly nonlinear profile, Figure 3(c), are the same for $F = 1.10$ and $L = 1.00$. Figure 3(b) is the nonlinear phase trajectory for Figure 3(a). This provides a check that our analysis of the weakly nonlinear phase plane (η, η_x) is correct. Analysis of the phase plane Figure 3(d) can help us understand these solutions and determine the number of independent parameters. We start to move from the saddle point $\eta = 0$, $\eta_x = 0$, in a clockwise direction on the solitary wave orbit, $C = 0$, past the maximum elevation $\eta = 2(F - 1)$, $\eta_x = 0$, before returning to the saddle point (see Figure 3(d)). The point $\eta = 2(F - 1)$, $\eta_x = 0$ in the weakly nonlinear phase plane represents the horizontal surfboard of arbitrary length L. Hence, for a given value of $F > 1$, the elevation of the horizontal board $\gamma = 2(F-1)$ comes as part of the solution and we are free to choose the length L of the surfboard. Therefore there is a two parameter family of solutions for $\sigma_c = 0$. Here the parameters are $F$and L.

We confirmed this understanding of the phase plane by computing nonlinear profiles for same value of $F = 1.10$ and different lengths L, of the horizontal surfboard. For $L = 0$ (i.e. solitary wave), $L = 1.00$ and $L = 2.00$ we obtained the same value of $\gamma = 0.21$.

We found that for values the Froude number $F > 1.15$ the differences between the weakly and nonlinear profiles were more noticeable. Further solutions for large values of F can be found in Vanden-Broeck & Keller [13].

We now consider supercritical flow, $F > 1$, past an inclined surfboard $\sigma_c \neq 0$. We recovered Vanden-Broeck & Keller's [13] one parameter family of nonlinear solutions. For a given value of the angle of inclination σ_c, the independent parameter can be chosen as the Froude number F. The elevation of the surfboard at the intersection with the upstream free surface γ, and the length of the board L, (or ϕ_c) came as part of the solution. Figure 4(a),(b) is a nonlinear profile and phase trajectory for $F = 1.10$, $\sigma_c = 2.3°$, $\gamma = 0.20$ and $L = 3.59$.

We also analytically derived a weakly nonlinear profile (see Figure 4(c)) for the same values of $F = 1.10$ and $\sigma_c = 2.3°$. The weakly nonlinear values of $\gamma = 0.18$ and $L = 3.05$ came as part of the solution. The nonlinear and weakly nonlinear profiles compare well in Figures 4(a),(c).

We now analyse the weakly nonlinear phase plane (Figure 4(d)) to determine the number of independent parameters to fix and give details of how the weakly nonlinear profile Figure 4(c) was derived.

For a given value of $F = 1.10$ we can graph the phase portrait Figure 4(d). Then a given value of σ_c determines the horizontal line $-\tan[\sigma_c]$ in the phase plane Figure 4(d). The elevation of the intersections of the surfboard with the upstream and downstream free surfaces, $\gamma = \eta_1$ and η_2 respectively, were determined as follows.

Using equation (2.36), $\frac{d\eta}{dx} = -\tan[\sigma_c]$ and $C = 0$, a cubic for η can be obtained

$$6(F-1)\eta^2 - 3\eta^3 = \tan[\sigma_c]^2. \tag{3.1}$$

We can define the three roots as $\eta_3 < \eta_2 < \eta_1$. The first root $\eta_1 = \gamma$ is then the elevation of the surfboard at the intersection with upstream free surface. The second root, η_2, is then the elevation of the surfboard at the intersection with downstream free surface. The length of the surfboard, $L = (\eta_1 - \eta_2)/\sin[\sigma_c]$, must then come as part of the solution, to ensure that the phase trajectory leaves and rejoins the solitary wave outer orbit in the phase plane Figure 4(d). We note that the third root, $\eta_3 < 0$, in (3.1) is no interest to us.

For values of $F = 1.30$ and $\sigma_c = 10.80°$ we computed a nonlinear solution and compared it to an analytically derived weakly nonlinear solution to establish the range of validity of the weakly nonlinear theory. We obtained the nonlinear values of $\gamma = 0.73$ and $L = 3.02$ which differs from the weakly nonlinear values of $\gamma = 0.56$ and $L = 2.10$. This is due to the fact that F is not close to 1. Qualitatively though, the free surface surface profiles are similar.

We now turn our attention to investigating subcritical flow, $F < 1$, past a horizontal or inclined plate of finite length.

3.2 Subcritical flows

We used the numerical scheme of § 2 in an attempt to compute fully nonlinear subcritical flows past a horizontal or inclined plate of finite length. We allowed a train of waves as $x \to -\infty$ and required the flow to be uniform as $x \to \infty$. If such a solution is obtained, we need to reverse the direction of the flow (i.e. the direction of the arrow in Figure 1(a)) to obtain a physically realistic flow satisfying the radiation condition.

We were not able to find any such solutions numerically. The nonexistence of these flows is consistent with the analysis of the weakly nonlinear phase plane in Figure 5(b). We note that there is now a saddle at $\eta = 4/3(F-1)$, $\eta_x = 0$ and a center at $\eta = 0$, $\eta_x = 0$. The horizontal plate can be represented by points on an inner periodic orbit (for example the bold one in Figure 5(b)), at the intersection with either the negative η-axis or positive η-axis. For Figure 5(a), $\gamma < 0$, and the horizontal board is therefore at the point where the bold inner periodic orbit intersects with the negative η-axis. To obtain a solution with constant depth as $x \to -\infty$ there would have to be a 'jump' off the bold inner periodic orbit into the centre at $\eta = 0$, $\eta_x = 0$ in the phase plane, see Figure 5(b). As there is no 'forcing' term in the KdV equation this simply cannot be achieved.

A similar analysis can be performed for subcritical flow past an inclined plate, see Figure 5(c)(d). Here the inclined plate is represented in Figure 5(c) by the horizontal line $\frac{d\eta}{dx} = -\tan[\sigma_c]$, joining the two inner periodic orbits in the phase plane Figure 5(d). There is no way to 'jump' from a periodic orbit into the centre $\eta = 0$, $\eta_x = 0$, in the phase plane, see Figure 5(d). Therefore, solutions are characterized by two trains of waves, upstream and downstream of the inclined surfboard, see Figure 5(d).

We have just established that in terms of the weakly nonlinear theory there can be no solutions that satisfy the radiation condition, for subcritical flow past a surfboard of finite length. We confirmed this understanding with our nonlinear theory and found no subcritical solutions that satisfied the radiation condition.

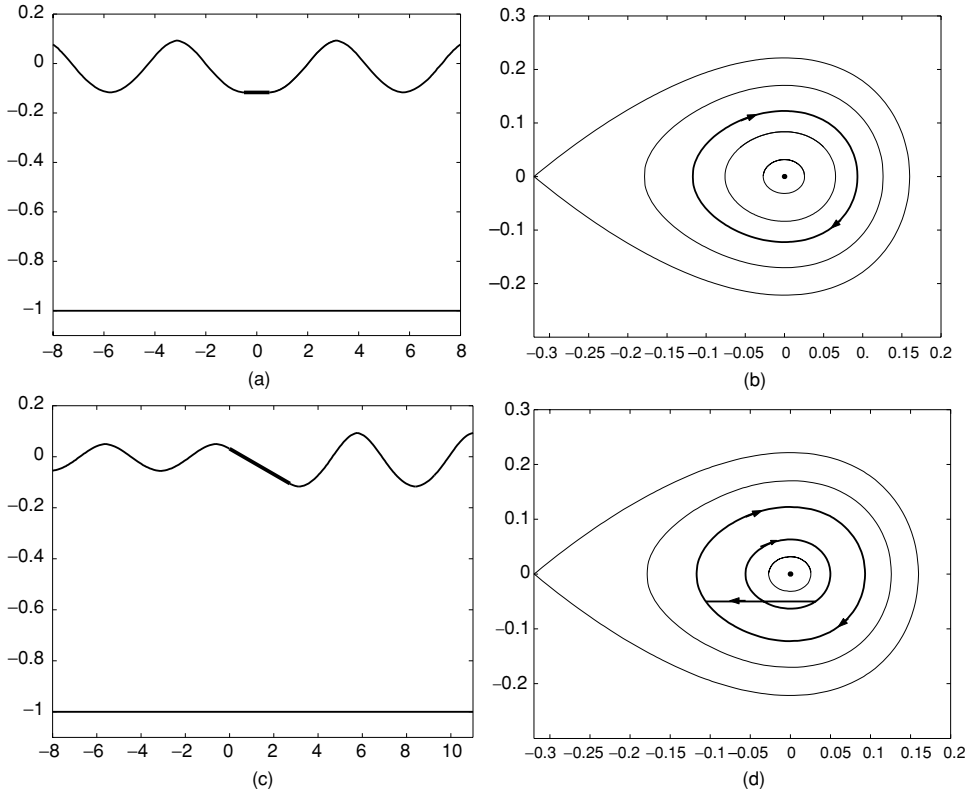

FIGURE 5. Subcritical flow for $F = 0.76$. (a) Weakly nonlinear profile, $\gamma = -0.12$, $\sigma_c = 0.0^\circ$ and $L = 1.00$. (b) Weakly nonlinear phase portrait for figure (a), $\frac{d\eta}{dx}$ versus η. (c) Weakly nonlinear profile, $\gamma = 0.031$, $\sigma_c = 2.86^\circ$ and $L = 2.74$. (d) Weakly nonlinear phase portrait for figure (c), $\frac{d\eta}{dx}$ versus η.

We have so far considered supercritical and subcritical flow past a rigid free surface obstruction (surfboard). In the next section we consider critical flow past an inclined sluice gate.

3.3 Flows under sluice gates

Flows under a sluice gate are defined by the configuration of Figure 1(a) with a uniform subcritical flow ($F^* < 1$) as $x \to -\infty$ and a uniform supercritical flow ($F > 1$) as $x \to \infty$.

Vanden-Broeck [14] solved numerically the flow for $\sigma_c = \pi/2$ and showed that there are no solutions with an uniform stream as $x \to -\infty$. All computed solutions have a train of waves as $x \to -\infty$. These solutions are not physical because the waves do not satisfy the radiation condition. In other words there are no sluice gate solutions for $\sigma_c = \pi/2$. Here we extend this result for $\sigma_c \neq \pi/2$. For $\sigma_c \ll \pi/2$, we can supplement the numerical computations by the weakly nonlinear theory and confirm that there is always a train of waves as $x \to -\infty$.

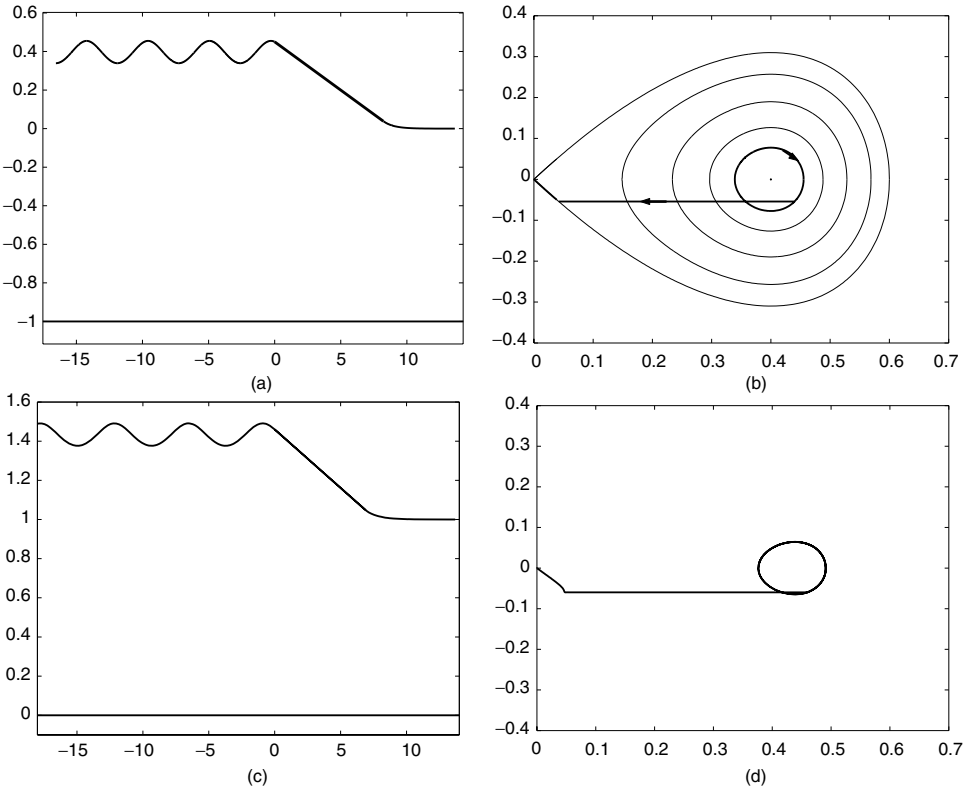

FIGURE 6. Critical flow for a value of the downstream Froude number, $F = 1.30$. (a) Weakly nonlinear free surface profile for values of $\sigma_c = 2.9°$, $\bar{\gamma} = 0.79$ and $L = 8.23$. (b) Weakly nonlinear phase portrait for figure (a), $\frac{d\eta}{dx}$ versus η. (c) Fully nonlinear free surface profile for values of $\sigma_c = 3.4°$, $\bar{\gamma} = 0.79$ and $L = 6.92$. (d) Values of $\frac{dy}{dx} = \tan(\theta)$ versus $y - 1 = \eta$, showing the fully nonlinear phase trajectories for Figure (c).

We specified the height of the intersection of the upstream free-surface with the gate as

$$y_1^U = y(0) = \left(1 + \frac{F^2}{2}\right)\bar{\gamma}$$

at $x = 0$. For flow separating tangentially from the gate at $x = 0$, $\bar{\gamma} < 1$. If there is a stagnation point at $x = 0$, $\bar{\gamma} = 1$.

We obtained numerically a three parameter family of nonlinear solutions with a train of waves on the upstream free surface. The three parameters were chosen as σ_c, F and $\bar{\gamma}$. The length of gate L (or ϕ_c) was found as part of the solution. These waves violate the radiation condition as $x \to -\infty$. Figures 6(c) and 7(a) are typical nonlinear profiles. No nonlinear solutions were obtained that satisfied (2.7) and the radiation condition as $x \to -\infty$.

Performing a weakly nonlinear analysis of the phase plane can determine the number of independent parameters and explain why there is no solution that satisfies the radiation condition, see Figure 6(b). For a given value of $F = 1.30$ the phase portrait can be plotted (Figure 6(b)) with a center at $\eta = 4/3(F - 1)$, $\eta_x = 0$ and saddle point at $\eta = 0$, $\eta_x = 0$.

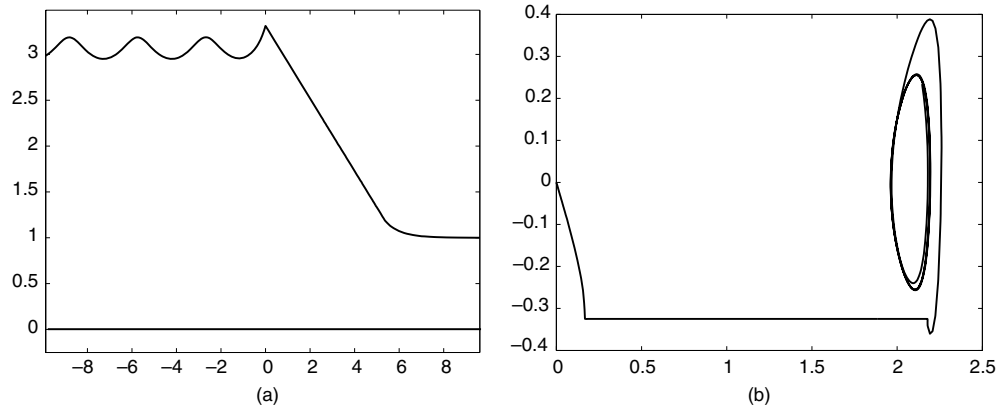

FIGURE 7. Critical flow, for $F = 2.15$ and $\sigma_c = 21.6°$. (a) Fully nonlinear free surface profile, $\bar{\gamma} = 0.98$, $L = 5.56$ and $\phi_c = 2.58$. (b) Values of $\frac{dy}{dx} = \tan(\theta)$ versus $y - 1 = \eta$, showing the fully nonlinear phase trajectories for Figure (a).

A given value of σ_c then determines the horizontal line, $\frac{d\eta}{dx} = -\tan[\sigma_c]$, in Figure 6(b). Fixing a value of $C = C_a$ in (2.36) then determines the inner periodic orbit or the amplitude of the waves.

The length of the gate L must then come as part of the solution to ensure that the horizontal line in Figure 6(b) joins the inner periodic orbit to the outer solitary wave orbit. Figure 6(a) is a weakly nonlinear profile for given values of $F = 1.30$, $\sigma_c = 2.9°$ and $\bar{\gamma} = 0.79$. Here we have viewed $\bar{\gamma}$ as the third parameter instead of C_a to be consistent with the nonlinear independent parameters. In Figure 6(c) we computed a nonlinear profile for the same values of $F = 1.30$ and $\bar{\gamma} = 0.79$ to compare with 6(a). Figure 6(d) is the nonlinear phase trajectory for Figure 6(c).

The phase plane analysis shows (Figure 6(b)) that there are no weakly nonlinear solutions that satisfy the radiation condition far upstream, for critical flow. This is because there can be no 'jump' from the center $\eta = 4/3(F - 1)$, $\eta_x = 0$, onto the horizontal line $\frac{d\eta}{dx} = -\tan[\sigma_c] \neq 0$, in the phase plane Figure 6(b).

We confirmed this new result in terms of the nonlinear theory by considering a given value of $\sigma_c = 15.3°$ and $F = 2.15$ for various values of $\bar{\gamma}$. We then plotted the amplitude of the waves (appearing on the upstream free surface) versus $\bar{\gamma}$, see Figure 8(b). Figure 8(b) illustrates that the amplitude of the waves can be decreased to a minimum $a_{min} \neq 0$. Similar results were obtained for other given values of the Froude number F and inclination σ_c, while varying $\bar{\gamma}$. Since $a_{min} > 0$ there are no waveless nonlinear solutions and the radiation condition is violated far upstream.

The effect of decreasing F, for a given angle of inclination, $\sigma_c = 21.6$, is shown in Figures 7(a) and 8(a). This result is qualitatively similar to that obtained by Vanden-Broeck [14] for the flow under a vertical sluice gate. As the Froude number is decreased, the amplitude of the waves increase and the profiles develop broad troughs and sharp crests. Ultimately they are expected to reach the Stokes limiting configuration of 120° angle at their crests.

Another Stokes limiting configuration with a stagnation point at the intersection of the upstream free-surface with the gate (at $x = 0$) is approached as $\bar{\gamma} \to 1$ in Figure 7(a).

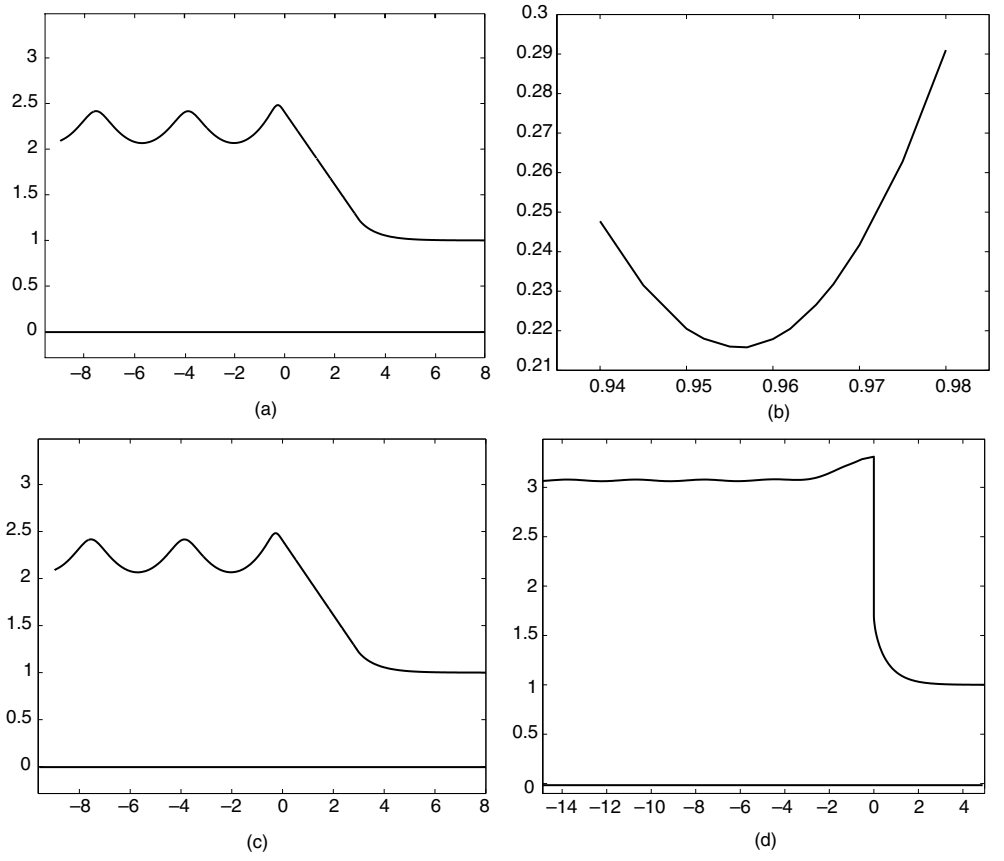

FIGURE 8. (a) Fully nonlinear free surface profile for $F = 1.75$, $\phi_c = 1.74$, $L = 3.20$, $\bar{\gamma} = 0.95$ and $\sigma_c = 21.6°$. (b) Graph of the wave amplitude a versus $\bar{\gamma}$, for a fixed value of $F = 2.15$ and $\sigma_c = 15.3°$. (c) Fully nonlinear free surface profile with a Stokes limiting configuration of 120° for a stagnation point at B. $F = 2.15$, $\phi_c = 2.57$, $\bar{\gamma} = 1.00$, $\sigma_c = 21.6°$ and $\theta_1^U = 38.4°$. (d) Fully nonlinear free surface profile for a vertical sluice gate, $F = 2.15$, $\phi_c = 0.31$, $\bar{\gamma} = 1.00$, $\theta_1^U = 0°$ and $\sigma_c = 90°$.

This limiting configuration can be computed directly by fixing $\bar{\gamma} = 1$ and imposing a 120° angle at $x = 0$, for $\sigma_c < 60°$, see Figure 8(c). (i.e. $\theta_1^U = 60° - \sigma_c$.) Notice that in Figure 7(a) the free surface is 'smooth' at the intersection of the gate with upstream free surface whereas in Figure 8(c) there is a slope discontinuity at $x = 0$.

Lastly, we consider the effect of varying the third parameter σ_c. For a given value of the Froude number $F = 2.15$ increasing the gate inclination σ_c decreases the amplitude of the waves appearing on the upstream free surface, see Figures 7(a), 8(c) and 8(d). Note that the amplitude of the waves in Figure 8(d) is small, but never equal to zero.

In Figure 8(d), we recover Vanden-Broeck's [14] solution for a vertical sluice gate ($\sigma_c = \pi/2$). This solution is outside the range of validity of the weakly nonlinear theory which assumes $\sigma_c \ll \pi/2$.

One way to derive models which satisfy the radiation condition is to replace the free surface AB by a rigid lid (see Budden & Norbury [5] and Asavanant & Vanden-Broeck [1]). Two such solutions are shown in Figure 9 for a vertical sluice gate. The top solid line

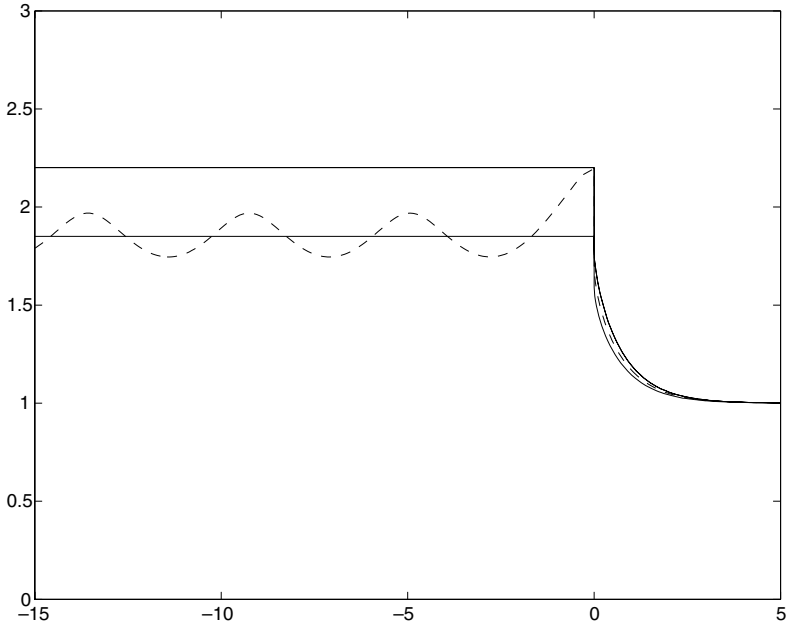

FIGURE 9. The solid curves are rigid lid approximations for a vertical sluice gate, $F = 1.55$. Top solid curve $\phi_c = 0.086$ and bottom solid curve $\phi_c = 0.051$. The broken curve is Vanden-Broeck's [14] recovered solution for a vertical sluice gate, $F = 1.55$ and $\phi_c = 0.073$.

corresponds to the choice $\bar{\gamma} = 1$. The bottom solid line is a better approximation in which $\bar{\gamma}$ was chosen so that the dynamic boundary condition (2.1) is satisfied as $x^* \to -\infty$. The broken line in Figure 9 is Vanden-Broeck's [14] wavy solution.

Another way to develop models which satisfy the radiation condition is to introduce an additional disturbance upstream. Such flows are not considered in this paper.

Finally, let us mention that solutions satisfying the radiation condition might be obtained by allowing a spray (or jet) at B (see for example Vanden-Broeck & Keller [13] and Dias & Vanden-Broeck [7]).

4 Conclusions

We have computed nonlinear free surface flows past surfboards and under sluice gates. Weakly nonlinear solutions were also derived analytically. We have shown that out of the six possible types of flows, only the supercritical flows, the subcritical flows with two trains of waves and the 'generalised critical' flows exist. The results imply in particular the nonexistence of subcritical flows satisfying the radiation condition. Similarly there are no solutions for the flow under a sluice gate that satisfy the radiation condition.

References

[1] ASAVANANT, J. & VANDEN-BROECK, J.-M. (1996) Nonlinear free-surface flows emerging from vessels and flows under a sluice gate. *J. Austal. Math. Soc.* **38**, 63–86.

[2] Benjamin, B. (1956) On the flow in channels when rigid obstacles are placed in the stream. *J. Fluid Mech.* **1**, 227–248.
[3] Binder, B. J., Dias, F. & Vanden-Broeck, J.-M. (2005) Forced solitary waves and fronts past submerged obstacles. *CHAOS*. (Submitted.)
[4] Binnie, A. M. (1952) The flow of water under a sluice gate. *Quart. J. Mech. Appl. Math.* **5**, 395–407.
[5] Budden, N. (1977) Sluice-gate problems with gravity. *Math. Proc. Camb. Phil. Soc.* **81**, 157–177.
[6] Chung, Y. K. (1972) Solution of flow under a sluice gates. *ASCE J. Eng. Mech. Div.* **98**, 121–140.
[7] Dias, F. & Vanden-Broeck, J.-M. (1993) Nonlinear bow flows with splashes. *J. Fluid Mech.* **255**, 91–102.
[8] Dias, F. & Vanden-Broeck, J.-M. (2002) Generalized critical free-surface flows. *J. Eng. Math.* **42**, 291–301.
[9] Frangmeier, D. D. & Strelkoff, T. S. (1968) Solution for gravity flow under a sluice gate. *ASCE J. Engng Mech. Div.* **94**, 153–176.
[10] Hocking, G. C. & Vanden-Broeck, J.-M. (1996) Draining of a fluid of finite depth into a slot. *Appl. Math. Mech. Modeling*. **94**.
[11] Larock, B. E. (1969) Gravity-affected flow from planar sluice gate. *ASCE J. Engng Mech. Div.* **96**, 1211–1226.
[12] Shen, S. S.-P. (1995) On the accuracy of the stationary forced Korteweg-de Vries equation as a model equation for flows over a bump. *Q. Appl. Math.* **53**, 701–719.
[13] Vanden-Broeck, J.-M. & Keller, J. B. (1989) Surfing on solitary waves. *J. Mech.* **198**, 115–125.
[14] Vanden-Broeck, J.-M. (1996) Numerical calculations of the free-surface flow under a sluice gate. *J. Fluid Mech.* **330**, 339–347.